arXiv:2205.06317v1 [cond-mat.supr-con] 12 May 2022

Tuning charge-density wave order and superconductivity in the kagome metals $KV_3Sb_{5-x}Sn_x$ and $RbV_3Sb_{5-x}Sn_x$

Yuzki M. Oey,[1] Farnaz Kaboudvand,[1] Brenden R. Ortiz,[1] Ram Seshadri,[1] and Stephen D. Wilson[1]

[1]*Materials Department, Materials Research Laboratory, and California NanoSystems Institute University of California Santa Barbara, California 93106 United States**

(Dated: May 16, 2022)

The family of AV_3Sb_5 (A = K, Rb, Cs) kagome metals exhibit charge density wave (CDW) order, proposed to be chiral, followed by a lower temperature superconducting state. Recent studies have proposed the importance of band structure saddle points proximal to the Fermi energy in governing these two transitions. Here we show the effects of hole-doping achieved *via* chemical substitution of Sn for Sb on the CDW and superconducting states in both KV_3Sb_5 and RbV_3Sb_5, and generate a phase diagram. Hole-doping lifts the Γ pocket and van Hove singularities (vHs) toward E_F causing the superconducting T_C in both systems to increase to about 4.5 K, while rapidly suppressing the CDW state.

INTRODUCTION

The AV_3Sb_5 (A: K, Rb, Cs) class of kagome superconductors [1–4] are proposed to host both unconventional CDW [5–7] and SC states [8–10] and are candidates for realizing these two states intertwined together within a host, pair density wave state [11–14]. One means of exploring this coupling is through chemical or mechanical perturbation of the host lattice and the parent electronic state of AV_3Sb_5 compounds. Recently, the effects of making small changes in the electronic band structures on SC and CDW order parameters have been studied computationally [15, 16] and experimentally by applying external hydrostatic pressure [17–20] and hole doping on various sites [21–23].

The electron pocket comprising Sb p_z orbitals at Γ and saddle points arising from V d-orbitals at M-points are regarded as playing important roles within the SC and CDW states. Consequently, resolving their behaviors when subject to external perturbations such as pressure and chemical doping is important to understand. Recently, the effect of hole doping in CsV_3Sb_5 with Sn substituting Sb was reported, and a double superconducting dome was observed under light hole-substitution [21]. The termination of the second dome was attributed to the lifting of the Γ pocket above E_F and the removal of the Sb p_z orbitals from the Fermi surface; however the formation of the first dome remains anomalous. Within the first SC dome, CDW order rapidly vanishes at doping levels corresponding to only slight movement of the the van Hove singularities (vHs) at the M point toward E_F [21]. Curiously, while applied external pressure moves the M saddle points away from E_F, it achieves a similar phase diagram suggesting a delicate balance of energy scales within the unperturbed parent structure [15, 18] and the dominance of removing the CDW state in governing the formation of the first SC dome.

In contrast to the above, pressure studies of KV_3Sb_5 and RbV_3Sb_5 have reported only a single superconducting dome coinciding with the suppression of CDW order [17, 19]; however studies of carrier-induced perturbations of these variants remain unexplored. To further explore similarities between pressure-induced and carrier-induced perturbations of the interplay between CDW and SC orders, here the effect of hole doping AV_3Sb_5 with in solid solutions with A = K, Rb is presented. In both systems, only one superconducting dome is observed in contrast with $CsV_3Sb_{5-x}Sn_x$, although a similar, rapid CDW suppression is observed. The solubility limit of Sn in KV_3Sb_5 is the lowest in the family, with phase separation observed by $x = 0.30$. In contrast RbV_3Sb_5 supports up to $x = 0.70$ of Sn replacing Sb. While the differences in solubility can be explained by A cation size effects, the difference between the single dome hole-doping phase diagrams of KV_3Sb_5 and RbV_3Sb_5 relative to double dome phase diagram of CsV_3Sb_5 suggests a difference in the parent CDW state between the three materials. The potential origins of these differences are discussed.

EXPERIMENTAL DETAILS

Powder samples of $KV_3Sb_{5-x}Sn_x$ and $RbV_3Sb_{5-x}Sn_x$ for $0 \leq x \leq 1$ were synthesized as described previously [21]. Structural analysis was performed *via* a Panalytical Empyrean laboratory x-ray powder diffractometer. A Hitachi TM4000Plus scanning electron microscope (SEM) was used to perform energy–dispersive X–ray spectroscopy (EDS). A Quantum Design Magnetic Property Measurement System (MPMS) was used to collect magnetization data and a Quantum Design Physical Property Measurement System (PPMS) Dynacool was used for resistivity measurements. To gain insight into the electronic states of all compounds, first-principles calculations based on density functional theory (DFT) within the Vienna ab initio Simulation Package (VASP) were performed [24, 25].

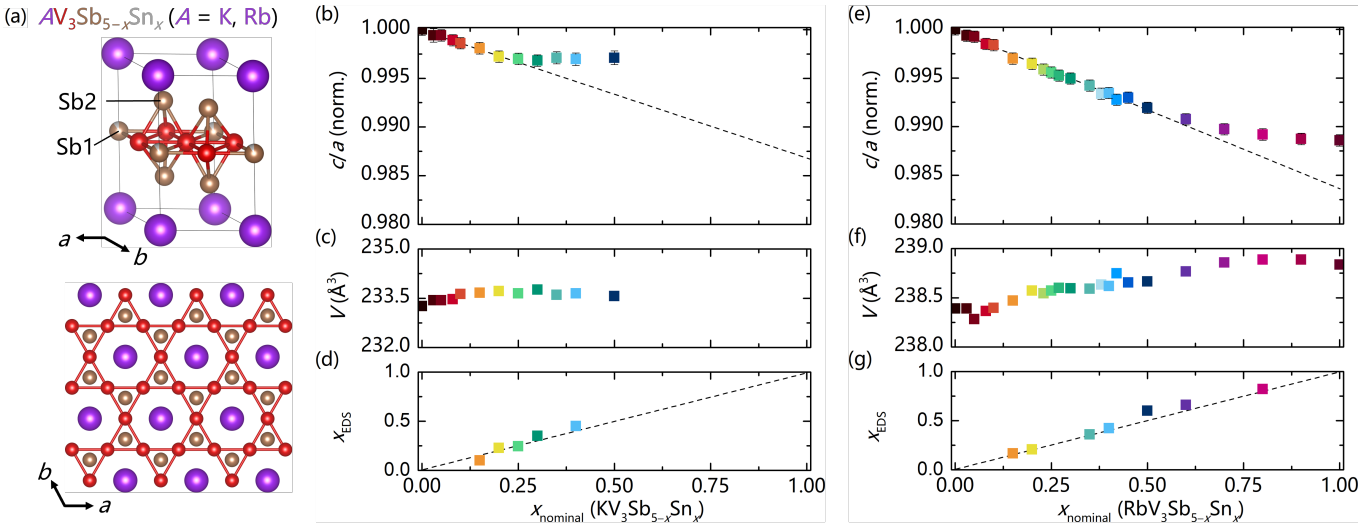


FIG. 1. (a) $AV_3Sb_{5-x}Sn_x$ crystallizes in the parent AV_3Sb_5 ($P6/mmm$) structure. Naively Sn can substitute on either the Sb1 or Sb2 sites, but from studies on $CsV_3Sb_{5-x}Sn_x$ it is clear that Sn preferentially substitutes in the in-plane kagome Sb1. (b-c) Sn integration into $KV_3Sb_{5-x}Sn_x$ causes the c/a ratio to decrease, and the solubility limit of Sn is $x \approx 0.25$, at which point the c/a ratio deviates from the linear trend. (e-f) The solubility limit of Sn in $RbV_3Sb_{5-x}Sn_x$ is a bit higher, at $x \approx 0.70$. (d, g) For samples with concentrations above the EDS sensitivity threshold, nominal Sn and measured Sn content agree. Error bars are shown unless they are smaller than associated point size.

EXPERIMENTAL AND COMPUTATIONAL RESULTS

$AV_3Sb_{5-x}Sn_x$ all adopt the parent hexagonal $P6/mmm$ structure at room temperature, with the V atoms making up an ideal kagome network. ^{121}Sb nuclear quadrupole resonance (NQR) studies on $CsV_3Sb_{5-x}Sn_x$ have shown that the Sn atoms preferentially occupy the Sb1 sublattice site in the kagome plane [21]. Due to the similarity in structure in all of the AV_3Sb_5 compounds, we assume that the Sn atoms occupy the Sb1 sublattice for A = K, Rb as well. For $KV_3Sb_{5-x}Sn_x$, polycrystalline samples were found to be single phase for $x \leq 0.25$, while for $RbV_3Sb_{5-x}Sn_x$, polycrystalline samples were single phase for $x \leq 0.7$, at which point the limit of the solid solution was reached and secondary phases were observed in both families.

Powder diffraction data were fitted using the Pawley method to study changes in unit cell as a function of Sn content. Similar to the changes observed in $CsV_3Sb_{5-x}Sn_x$, a increases as c decreases with increasing Sn content in both A = K, Rb as seen in Fig. 1(b,e), while the volume is independent of Sn content (Fig. 1(c,f)). The solubility limit of Sn is clearly reached once the c/a ratio deviates from its linear trend ($x \approx 0.30$ for $KV_3Sb_{5-x}Sn_x$ and $x \approx 0.70$ for $RbV_3Sb_{5-x}Sn_x$), and a secondary phase emerges in the powder diffraction data. EDS was performed on samples with a critical Sn content to confirm the nominal Sn content (Fig. 1(d, g)).

Single crystal KV_3Sb_5 has a superconducting T_C of 0.93 K[3]. Here, the T_C of polycrystalline KV_3Sb_5 is lower than 1.8 K, the lowest achievable temperature on the MPMS, but as Sn was incorporated, the superconducting transition temperature increases and can be detected by $x = 0.03$. Figure 2(a) shows the evolution of the superconducting transition up to $x = 0.25$, where T_C is at a maximum of 4.5 K. Beyond this Sn content, a secondary phase appears, so an eventual suppression of superconductivity is not observed within the solid solution of $KV_3Sb_{5-x}Sn_x$. RbV_3Sb_5 shows similar behavior, with undoped crystals showing a T_C of 0.92 K[26]. Again, although the superconducting transition for RbV_3Sb_5 cannot be detected with an MPMS, by $x = 0.05$ the transition appears at 1.93 K and increases to a maximum of 4.5 K for $x = 0.40$, as seen in Figure 2(c). For $x > 0.40$, T_C decreases to 3.55 K until a clear secondary phase appears. All of the superconducting volume fractions are approximately $4\pi\chi_v \approx -1$ and are normalized to -1 for ease of comparison; fractions that deviate slightly from this ideal value can be attributed to errors in packing density.

The CDW T^* was determined by looking at the inflection point of χ^{-1} *vs.* T. Polycrystalline KV_3Sb_5 as observed here has a T^* of 86 K, which is in good agreement with reported CDW transition temperatures of $\approx$ 80 K in crystals [4]. Using this metric, the CDW transition is quickly suppressed with increasing hole-doping, decreases to 60 K by $x = 0.06$, and is fully suppressed by $x = 0.06$. In RbV_3Sb_5, the CDW T^* using the same metric is $\approx$ 112 K, similar to the literature reported value [1]. The CDW is quickly suppressed to 91 K for $x = 0.10$ at which point it fully disappears (Fig. 2(d)). In both systems, the CDW transition is fully suppressed with much less Sn content than that required to reach the peak of

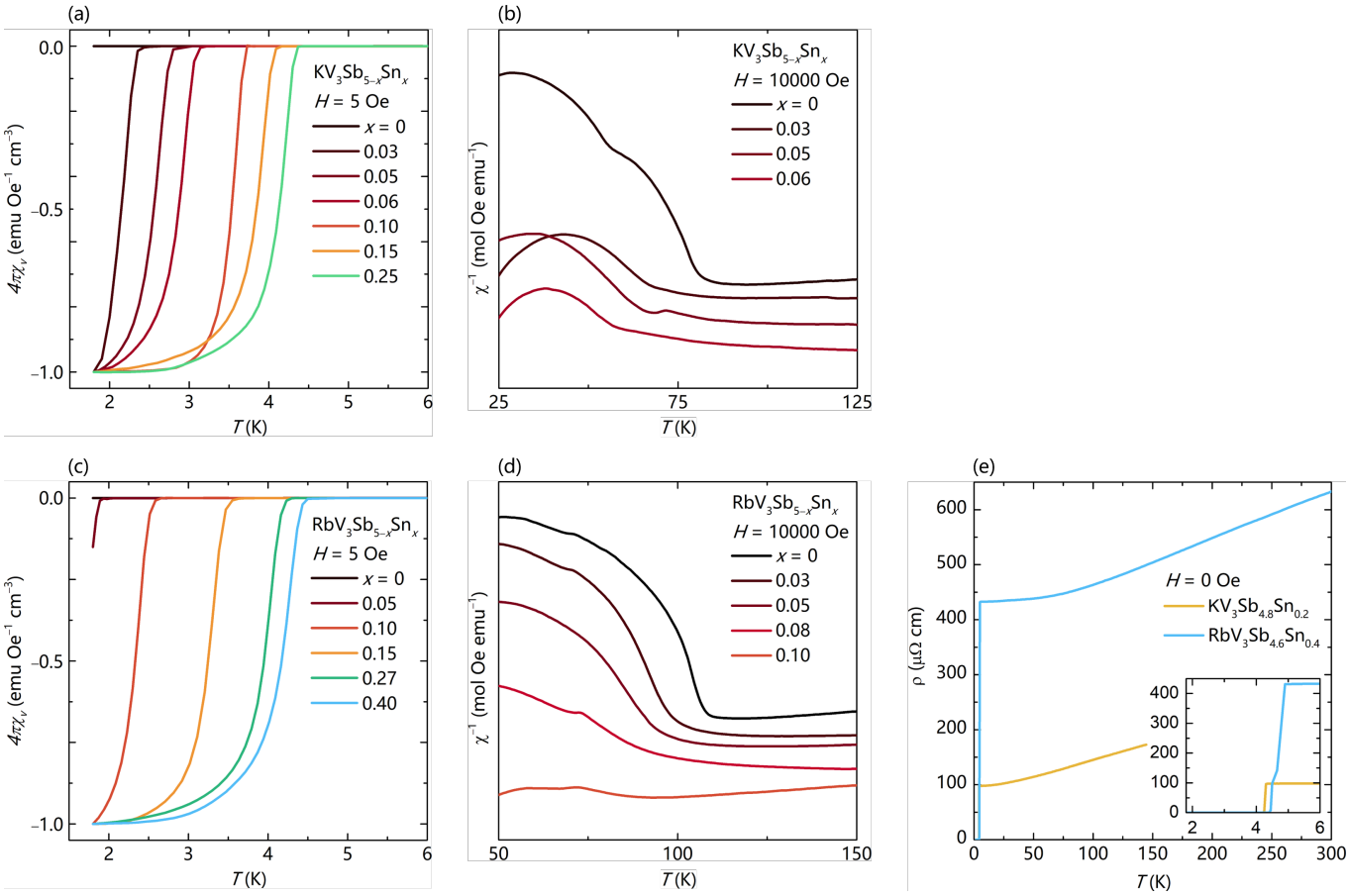


FIG. 2. (a) The superconducting T_C of $KV_3Sb_{5-x}Sn_x$ measured under a field of $H = 5$ Oe systematically shifts to higher temperature in compositions up to $x = 0.30$. The superconducting fraction is normalized to account for errors in mass and packing fraction so all data have a minimum of -1, the theoretical minimum. (b) $1/\chi$ for compositions $x \leq 0.05$ in $KV_3Sb_{5-x}Sn_x$ show the CDW T^* decreases from 86 K to 59 K and disappears for $x \geq 0.05$. (c) The superconducting T_C of $RbV_3Sb_{5-x}Sn_x$ measured under a field of $H = 5$ Oe systematically shifts to higher temperature in compositions up to $x = 0.40$. (d) $1/\chi$ for compositions $x \leq 0.10$ in $RbV_3Sb_{5-x}Sn_x$ show the CDW T^* decreases and eventually disappears for $x \geq 0.10$. (e) Resistivity data for $KV_3Sb_{4.8}Sn_{0.2}$ and $RbV_3Sb_{4.6}Sn_{0.4}$ confirm the T_C transitions and lack of CDW transitions for these higher Sn content samples.

the superconductivity dome, suggesting that the interplay between superconductivity and CDW is different in A = K, Rb than in CsV_3Sb_5, where the CDW persists through the peak of the first superconducting dome.

Electrical resistivity measurements of samples near the superconducting peak concentrations are shown in Figure 2(e). The superconducting states are clearly observed as zero-resistivity conditions and the transitions at 4.25 K for $KV_3Sb_{4.80}Sn_{0.20}$ and 4.4 K for $RbV_3Sb_{4.60}Sn_{0.40}$ agree well with those seen in the magnetization data, while signatures of CDW transitions are also not present. Consistent with $CsV_3Sb_{5-x}Sn_x$, the residual resistance increases in $RbV_3Sb_{5-x}Sn_x$ and $KV_3Sb_{5-x}Sn_x$ under Sn-substitution while T_C increases.

The effects of Sn-substitution on SC and CDW orders in $KV_3Sb_{5-x}Sn_x$ and $RbV_3Sb_{5-x}Sn_x$ are summarized in Figure 3. In both systems, the CDW ordering temperature is rapidly suppressed with small levels of hole doping and fully disappears before the maximum superconducting transition temperatures. With the exception of the soluability limit of Sn in each lattice, the two phase diagrams are qualitatively similar.

Due to size considerations, the solubility limits of Sn in KV_3Sb_5 and RbV_3Sb_5 are much lower than in CsV_3Sb_5. However in all of these systems, the changes in electronic structure for the compositions of interest can be extrapolated by computing band structures of substitution one Sb atom for an Sn atom within the kagome plane and out of the kagome plane. Figure 4(a) and (d) shows the band structure of undoped KV_3Sb_5 and RbV_3Sb_5, respectively, with the range of achievable Fermi levels with the loss of 1 electron per unit cell indicated in gray. Figure 4(b) and (e) show a hypothetical structure where the Sb1 lattice is fully substituted for Sn. The shifts in band structure are similar to those seen in CsV_3Sb_4Sn, with the Γ pocket and M-point vHs lifted above the Fermi level.

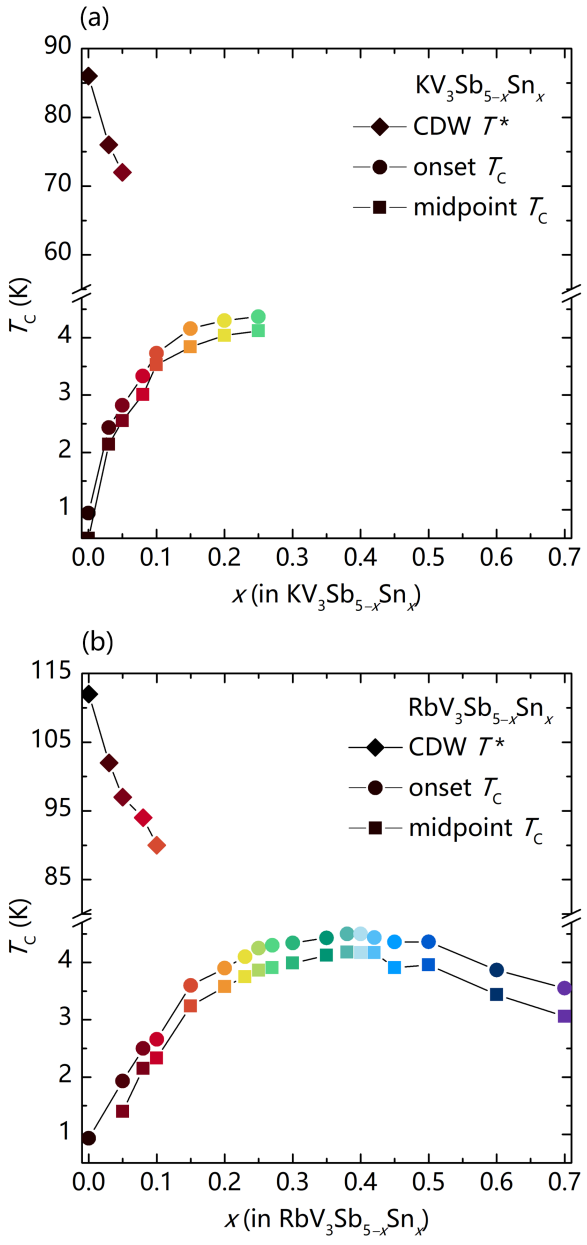


FIG. 3. The progression of superconducting T_C and CDW order T^* is plotted as a function of Sn composition for $KV_3Sb_{5-x}Sn_x$ and $RbV_3Sb_{5-x}Sn_x$. In $KV_3Sb_{5-x}Sn_x$, the solubility limit of Sn is reached before a full superconducting dome is achieved, but the suppression of CDW T^* is still fully realized. $RbV_3Sb_{5-x}Sn_x$ shows a single superconducting dome before the solubility limit is reached, with an accompanying suppression of CDW order by $x = 0.1$.

Band structures for Sn substituted within the Sb2 sublattice are plotted in Figure 4(c) and (f) and show significant reconstructions at multiple points, including K, L, and H.

DISCUSSION

Given the close structural and electronic properties across the AV_3Sb_5 series, the difference in the hole-doping phase diagrams of KV_3Sb_5 and RbV_3Sb_5 relative to CsV_3Sb_5 is anomalous. The changes in band structure for Sn substitution on the Sb1 sublattice in KV_3Sb_4Sn and RbV_3Sb_4Sn at first sight, appear to be very similar to those in CsV_3Sb_4Sn. However, subtle differences are nevertheless present and potentially lead to distinct electronic phase diagrams. A closer examination of the saddle points around M reveals that the irreducible representations of the two points are not the same for A = K, Rb and Cs [15, 16]. As a consequence of the saddle point inversions, bands cross near E_F in CsV_3Sb_5 but not in KV_3Sb_5. This may play a role in the nature of the CDW states stabilized, whose proximity to one another may modify SC in unique ways.

One unifying theme amongst doping and pressure studies of AV_3Sb_5 is the similarity of two SC domes present uniquely in CsV_3Sb_5. If one envisions either pressure/doping empirically as a perturbation that simply destabilizes CDW order, then the data suggest that CsV_3Sb_5 hosts a CDW state distinct from the other two variants. In this scenario, there is a transition between CDW states within the phase diagram of CsV_3Sb_5 that is naively absent in KV_3Sb_5 and RbV_3Sb_5.

While the details of the intermediate states differ between pressure and hole-doping studies, investigations of the parent CDW order in AV_3Sb_5 have shown differences between A=Cs and A =Rb/K. The out-of-plane modulation for Cs is four times that of K [4, 27], and the in-plane structure of the CDW state in CsV_3Sb_5 hosts both star-of-David and tri-hexagonal character [27–29], a pattern seemingly not present in the other variants. Given these differences, one possibility is a doping-induced transition from an (L, L, L)-type order to an (M, L, L)-type of order upon doping CsV_3Sb_5 [30] that is not present in the other two compounds. Future scattering studies across the carrier-tuned phase diagrams of these systems will be required to fully explore any potential crossover.

CONCLUSION

The Sn-substitution or hole-doping phase diagrams of KV_3Sb_5 and RbV_3Sb_5 were explored. The solubility of Sn within the AV_3Sb_5 lattice varies with A-site cation size with A=K having the smallest solubility and A=Cs having the largest. Prior to reaching the solubility limit, hole-doping achieved *via* substitution of Sn on Sb sites in KV_3Sb_5 and RbV_3Sb_5 reveals similar phase diagrams consisting of a single SC dome and rapidly suppressed CDW order. This contrasts the recently reported double dome observed in CsV_3Sb_5 and suggests a distinct parent

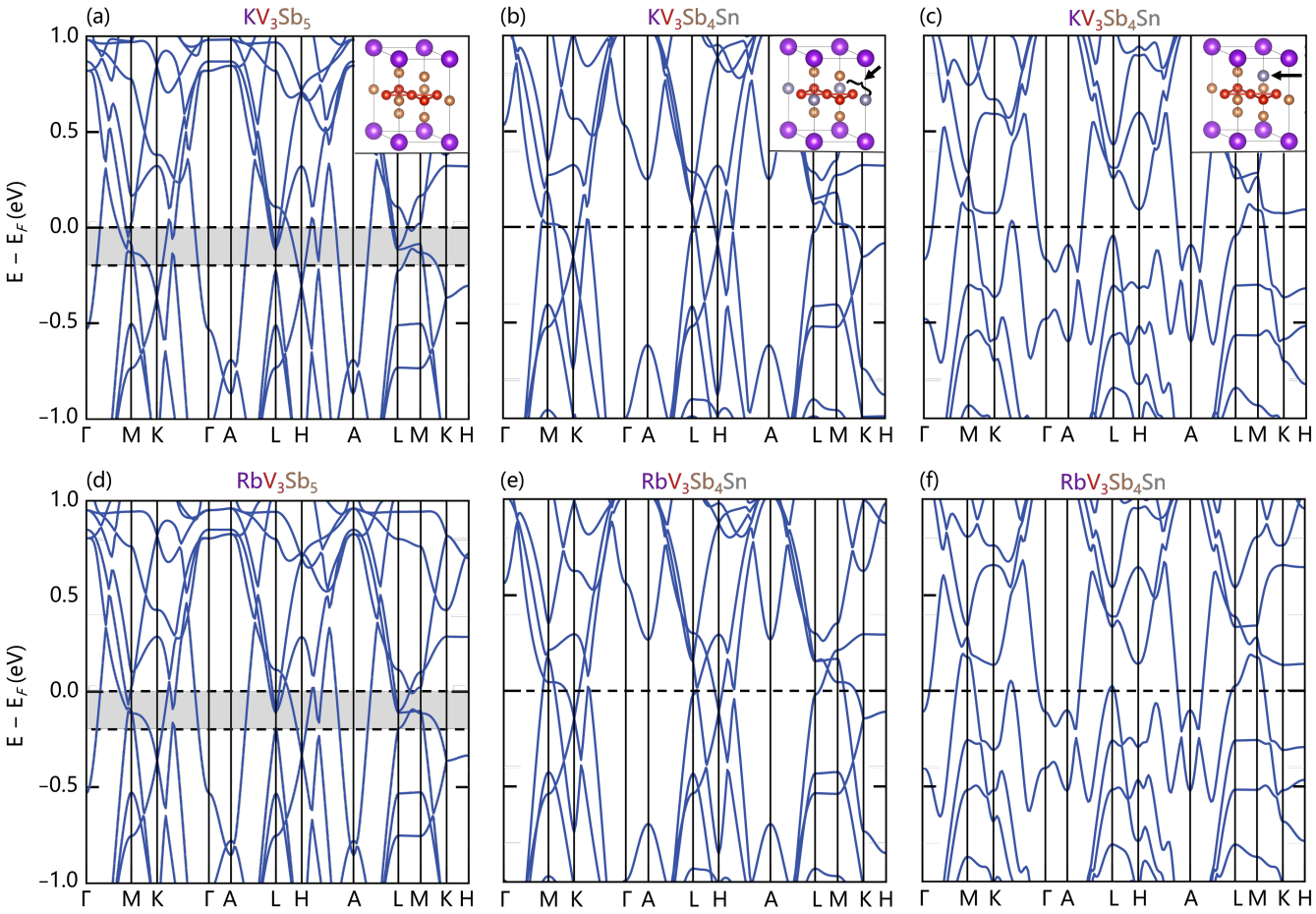


FIG. 4. (a,d) DFT calculations for KV_3Sb_5 and RbV_3Sb_5 highlighting the allowable range of Fermi levels under the rigid band approximation for substitution of one Sn atom per formula unit (one electron less Fermi energy). (b,e) Calculation for a hypothetical structure where one Sn has been substituted within the kagome plan (Sb1 sublattice). The majority of the electronic structure is preserved as KV_3Sb_5 and RbV_3Sb_5, except the Γ pocket and M point van Hove singularities which have been shifted far above and may contribute to the changing observable properties. (c,f) Calculation for a hypothetical structure where one Sn has been substituted out of the kagome plane (Sb2 sublattice). Here a strong reconstruction of many bands can be observed, in particular near K, H, and K-Γ.

CDW state for the latter.

ACKNOWLEDGMENTS

This work was supported by the National Science Foundation (NSF) through Enabling Quantum Leap: Convergent Accelerated Discovery Foundries for Quantum Materials Science, Engineering and Information (Q-AMASE-i): Quantum Foundry at UC Santa Barbara (DMR-1906325). The research reported here made use of shared facilities of the NSF Materials Research Science and Engineering Center at UC Santa Barbara DMR-1720256, a member of the Materials Research Facilities Network (www.mrfn.org). Use of the Advanced Photon Source at Argonne National Laboratory was supported by the U.S. Department of Energy, Office of Science, Office of Basic Energy Sciences, under Contract No. DE-AC02-06CH11357. YMO is supported by the National Science Foundation Graduate Research Fellowship Program under Grant No. DGE-1650114. FK acknowledges the Roy T. Eddleman Center for Quantum Innovation (ECQI) for their support.

REFERENCES

* yoey@ucsb.edu

[1] B. R. Ortiz, L. C. Gomes, J. R. Morey, M. Winiarski, M. Bordelon, J. S. Mangum, I. W. Oswald, J. A. Rodriguez-Rivera, J. R. Neilson, S. D. Wilson, *et al.*, New kagome

prototype materials: discovery of KV_3Sb_5, RbV_3Sb_5, and CsV_3Sb_5, Phys. Rev. Mater. **3**, 094407 (2019).

[2] B. R. Ortiz, S. M. Teicher, Y. Hu, J. L. Zuo, P. M. Sarte, E. C. Schueller, A. M. Abeykoon, M. J. Krogstad, S. Rosenkranz, R. Osborn, R. Seshadri, L. Balents, J. He, and S. D. Wilson, CsV_3Sb_5: A $\mathbb{Z}_2$ topological kagome metal with a superconducting ground state, Phys. Rev, Lett. **125**, 247002 (2020).

[3] B. R. Ortiz, P. M. Sarte, E. M. Kenney, M. J. Graf, S. M. Teicher, R. Seshadri, and S. D. Wilson, Superconductivity in the $\mathbb{Z}_2$ kagome metal KV_3Sb_5, Phys. Rev. Mater. **5**, 034801 (2021).

[4] Y.-X. Jiang, J.-X. Yin, M. M. Denner, N. Shumiya, B. R. Ortiz, G. Xu, Z. Guguchia, J. He, M. S. Hossain, X. Liu, *et al.*, Unconventional chiral charge order in kagome superconductor KV_3Sb_5, Nat. Mater. , 1 (2021).

[5] X. Feng, Y. Zhang, K. Jiang, and J. Hu, Low-energy effective theory and symmetry classification of flux phases on the kagome lattice, Phys. Rev. B **104**, 165136 (2021).

[6] T. Park, M. Ye, and L. Balents, Electronic instabilities of kagome metals: saddle points and landau theory, Phys. Rev. B **104**, 035142 (2021).

[7] Y.-P. Lin and R. M. Nandkishore, Complex charge density waves at Van Hove singularity on hexagonal lattices: Haldane-model phase diagram and potential realization in the kagome metals AV_3Sb_5 (A= K, Rb, Cs), Phys. Rev. B **104**, 045122 (2021).

[8] M. L. Kiesel, C. Platt, and R. Thomale, Unconventional fermi surface instabilities in the kagome Hubbard model, Phys. Rev. Lett. **110**, 126405 (2013).

[9] X. Wu, T. Schwemmer, T. Müller, A. Consiglio, G. Sangiovanni, D. Di Sante, Y. Iqbal, W. Hanke, A. P. Schnyder, M. M. Denner, *et al.*, Nature of Unconventional Pairing in the Kagome Superconductors AV_3Sb_5 (A= K, Rb, Cs), Phys. Rev. Lett. **127**, 177001 (2021).

[10] Y.-P. Lin and R. M. Nandkishore, Kagome superconductors from Pomeranchuk fluctuations in charge density wave metals, arXiv preprint arXiv:2107.09050 (2021).

[11] H. Chen, H. Yang, B. Hu, Z. Zhao, J. Yuan, Y. Xing, G. Qian, Z. Huang, G. Li, Y. Ye, *et al.*, Roton pair density wave in a strong-coupling kagome superconductor, Nature **599**, 222 (2021).

[12] J. Ge, P. Wang, Y. Xing, Q. Yin, H. Lei, Z. Wang, and J. Wang, Discovery of charge-4e and charge-6e superconductivity in kagome superconductor CsV_3Sb_5, arXiv preprint arXiv:2201.10352 (2022).

[13] D. F. Agterberg, M. Geracie, and H. Tsunetsugu, Conventional and charge-six superfluids from melting hexagonal Fulde-Ferrell-Larkin-Ovchinnikov phases in two dimensions, Phys. Rev. B **84**, 014513 (2011).

[14] S. Zhou and Z. Wang, Chern Fermi-pockets and chiral topological pair density waves in kagome superconductors, arXiv preprint arXiv:2110.06266 (2021).

[15] H. LaBollita and A. S. Botana, Tuning the Van Hove singularities in AV_3Sb_5 (A= K, Rb, Cs) via pressure and doping, Physical Review B **104**, 205129 (2021).

[16] E. Uykur, B. Ortiz, O. Iakutkina, M. Wenzel, S. Wilson, M. Dressel, and A. Tsirlin, Low-energy optical properties of the nonmagnetic kagome metal CsV_3Sb_5, Physical Review B **104**, 045130 (2021).

[17] F. Du, S. Luo, B. R. Ortiz, Y. Chen, W. Duan, D. Zhang, X. Lu, S. D. Wilson, Y. Song, and H. Yuan, Pressure-induced double superconducting domes and charge instability in the kagome metal KV_3Sb_5, Phys. Rev. B **103**, L220504 (2021).

[18] K. Chen, N. Wang, Q. Yin, Y. Gu, K. Jiang, Z. Tu, C. Gong, Y. Uwatoko, J. Sun, H. Lei, *et al.*, Double superconducting dome and triple enhancement of T_C in the kagome superconductor CsV_3Sb_5 under high pressure, Phys. Rev. Lett. **126**, 247001 (2021).

[19] C. Zhu, X. Yang, W. Xia, Q. Yin, L. Wang, C. Zhao, D. Dai, C. Tu, B. Song, Z. Tao, *et al.*, Double-dome superconductivity under pressure in the V-based kagome metals AV_3Sb_5 (A = Rb and K), Phys. Rev. B **105**, 094507 (2022).

[20] F. Yu, D. Ma, W. Zhuo, S. Liu, X. Wen, B. Lei, J. Ying, and X. Chen, Unusual competition of superconductivity and charge-density-wave state in a compressed topological kagome metal, Nat. Commun. **12**, 1 (2021).

[21] Y. M. Oey, B. R. Ortiz, F. Kaboudvand, J. Frassineti, E. Garcia, S. Sanna, V. Mitrović, R. Seshadri, and S. D. Wilson, Fermi level tuning and double-dome superconductivity in the kagome metals $CsV_3Sb_{5-x}Sn_x$, Phys. Rev. Mater. **6** (2022).

[22] H. Yang, Y. Zhang, Z. Huang, Z. Zhao, J. Shi, G. Qian, B. Hu, Z. Lu, H. Zhang, C. Shen, *et al.*, Doping and two distinct phases in strong-coupling kagome superconductors, arXiv preprint arXiv:2110.11228 (2021).

[23] Y. Liu, Y. Wang, Y. Cai, Z. Hao, X.-M. Ma, L. Wang, C. Liu, J. Chen, L. Zhou, J. Wang, *et al.*, Doping evolution of superconductivity, charge order and band topology in hole-doped topological kagome superconductors $Cs(V_{1-x}Ti_x)_3Sb_5$, arXiv preprint arXiv:2110.12651 (2021).

[24] G. Kresse and J. Furthmüller, Efficient iterative schemes for ab initio total-energy calculations using a plane-wave basis set, Phys. Rev. B **54**, 11169 (1996).

[25] G. Kresse and J. Furthmüller, Efficiency of ab-initio total energy calculations for metals and semiconductors using a plane-wave basis set, Comput. Mater. Sci. **6**, 15 (1996).

[26] Q. Yin, Z. Tu, C. Gong, Y. Fu, S. Yan, and H. Lei, Superconductivity and normal-state properties of kagome metal RbV_3Sb_5 single crystals, Chinese Phys. Lett. **38**, 037403 (2021).

[27] B. R. Ortiz, S. M. Teicher, L. Kautzsch, P. M. Sarte, N. Ratcliff, J. Harter, J. P. Ruff, R. Seshadri, and S. D. Wilson, Fermi surface mapping and the nature of charge density wave order in the kagome superconductor CsV_3Sb_5, Phys. Rev. X **11**, 041030 (2021).

[28] Y. Hu, X. Wu, B. R. Ortiz, X. Han, N. C. Plumb, S. D. Wilson, A. P. Schnyder, and M. Shi, Coexistence of Tri-Hexagonal and Star-of-David Pattern in the Charge Density Wave of the Kagome Superconductor AV_3Sb_5, arXiv preprint arXiv:2201.06477 (2022).

[29] M. Kang, S. Fang, J. Yoo, B. R. Ortiz, Y. Oey, S. H. Ryu, J. Kim, C. Jozwiak, A. Bostwick, E. Rotenberg, *et al.*, Microscopic structure of three-dimensional charge order in kagome superconductor av3sb5 and its tunability, arXiv preprint arXiv:2202.01902 (2022).

[30] M. H. Christensen, T. Birol, B. M. Andersen, and R. M. Fernandes, Theory of the charge density wave in AV_3Sb_5 kagome metals, Phys. Rev. B **104**, 214513 (2021).